Green Chemistry

PAPER

View Article Online
View Journal | View Issue

Cite this: *Green Chem.*, 2023, **25**, 5741

Structure–activity relationships of LDH catalysts for the glucose-to-fructose isomerisation in ethanol†

Krisztina Karádi,[a] Thanh-Truc Nguyen,[b] Adél Anna Ádám,[a] Kornélia Baán,[c] András Sápi,[c] Ákos Kukovecz,[c] Zoltán Kónya,[c] Pál Sipos,*[d] István Pálinkó‡[a] and Gábor Varga*§[e]

Glucose-to-fructose isomerization is the key process in the reaction sequence that can lead to the total conversion of biomass into valuable fine chemicals. However, it is challenging to find an efficient, cost-effective- and waste-minimized process to produce High Fructose Corn Syrup (HFCS) without using non-green approaches. To this end, hydrotalcite (MgAl-layered double hydroxides (MgAl-LDH)) catalyzed glucose isomerization in ethanol seemed to be one of the most promising processes in the last decade. In contrast to the well-studied reaction carried out in aqueous solutions, when ethanolic solutions are used, many potentially important properties of the LDHs cannot be studied in terms of how they affect their own catalytic abilities. Neither the effect of the basic site distribution, nor the morphological aspects and the role of surface hydration have been elucidated so far. In this study, the systematic alteration of the textural and structural parameters of hydrotalcites and hydrocalumites (Ca_2Al-LDH) revealed clear structure–activity-selectivity relationships. These indicate that the rate-determining factor is the hydrophilicity and the LDH surface factors affecting it, which determine the catalytic performance of the LDH catalyst more than any other factor. This is evidenced by the fact that the catalytic efficiency of hydrotalcites can be improved by reducing their basicity. When isomerizations catalyzed by the easily recyclable LDH with suitable surface features are carried out, a truly similar catalytic performance (71% glucose conversion, 83% fructose selectivity, 59% fructose yield) can be achieved as was previously described, but at a significantly lower reaction temperature (120 °C → 80 °C).

Received 30th May 2023,
Accepted 29th June 2023

DOI: 10.1039/d3gc01860a

rsc.li/greenchem

1. Introduction

Glucose-to-fructose isomerization is the key process to produce High Fructose Corn Syrup (HFCS),[1] used in industry and also in academia,[2] especially for producing biofuels and platform molecules.[3,4] Moreover, this reaction is also well-known as a crucial step for the catalytic valorisation of the lignocellulose, which is attracting increasing global interest because of the depletion of fossil resources.[5–11] While industrial catalytic isomerizations have thus far largely utilized the high-performance isomerases as actual catalysts,[1,12] the newly developed catalytic systems are based on inorganic (nano)materials because of the strong limitations of the widely used enzymatic transformations. Particularly, both the low persistence and the separation of the enzymes from the liquor after the reaction have remained very challenging and costly.[13] In addition, fine-tuning of the catalysts, taking into account the variable feedstocks depending on the lignocellulose sources, proved to be impossible without giving rise to variations in their catalytic ability. Additionally, the maximum glucose conversions of 50% can be achieved by means of enzymatic catalysis because of thermodynamic reasons.[14,15] Furthermore, isomerases are

[a]*Department of Organic Chemistry and Materials and Solution Structure Research Group, University of Szeged, Dóm tér 8, Szeged, H-6720 Hungary*
[b]*Australian Institute for Bioengineering and Nanotechnology, The University of Queensland, Brisbane, QLD 4072, Australia*
[c]*Department of Applied and Environmental Chemistry and Interdisciplinary Excellence Centre, Institute of Chemistry, University of Szeged, Rerrich Béla tér 1, Szeged, H-6720 Hungary*
[d]*Department of Inorganic and Analytical Chemistry and Materials and Solution Structure Research Group, University of Szeged, Dóm tér 7, Szeged, H-6720 Hungary. E-mail: sipos@chem.u-szeged.hu*
[e]*Department of Physical Chemistry and Materials Science and Materials and Solution Structure Research Group, University of Szeged, Rerrich Béla tér 1, Szeged, H-6720 Hungary. E-mail: gabor.varga5@chem.u-szeged.hu*

† Electronic supplementary information (ESI) available: Detailed experimental part; representative BET isotherms; XRD patterns of the heat-treated and rehydrated Mg_3Al- and Mg_4Al-LDHs, nitrate- and chloride-containing hydrotalcites and fresh, treated and spent hydrocalumites; CO_2-TPD profiles of calcined hydrotalcites; plot of the total number of basic sites for heat-treated and rehydrated Mg_3Al-LDH and Mg_4Al- as well as Ca_2Al-LDHs; SEM images of calcined and calcined-rehydrated Mg_3Al-LDH and Mg_4Al-LDHs; catalytic performance of the as-prepared and treated Mg_3Al-LDHs; basicity, composition and crystallographic data. See DOI: https://doi.org/10.1039/d3gc01860a

‡ Passed away.

§ Present address: Australian Institute for Bioengineering and Nanotechnology, The University of Queensland, Brisbane, QLD 4072, Australia.

mainly obtained from genetically modified strains, by now, being under close regulation of, *e.g.*, the European Union.[16]

However, thermal catalysis has means of displacing enzymatic isomerizations; particularly, two alternative reaction pathways are also known. Among them, the Lewis acid catalyzed intermolecular hydride shift seems to be the more efficient in terms of glucose conversion.[17,18] But this has strong limitations in its robustness and selectivity due to the completion of the side reactions such as intramolecular carbon shift.[17] Although lower conversion rates can be achieved *via* the Brønsted base catalyzed keto–enol tautomerization, which is the so-called Lobry de Bruyn–Alberda van Ekenstein rearrangement,[19] unique selectivity of these catalytic processes toward fructose is possible to be obtained that has made it a possible alternative to enzyme catalysed processes.[20] Hence, the application of pure inorganic bases seems to be obvious, by its very nature, inorganic bases such as alkali hydroxides have already been tested as actual catalysts under homogenous catalytic conditions and each one proved to be highly active.[21,22] For example, upon using NaOH, up to glucose conversion of 66% can be achieved.[23] The application of strongly alkaline medium and the strong basicity of the catalysts led to the degradation of monosaccharides – in parallel with the decrease of the fructose selectivity (~maximum value of 10%) – that produced approximately 50 different by-products, particularly, carboxylic acid derivatives.[24] In order to address these problems in the fructose-selectivity, catalytically active organic amines and organic bases were used, presenting almost exclusive fructose-selectivity, however, with poor glucose conversions (~30%).[24–27] The reduced glucose conversion was mainly due to the reversibility of the isomerization. To shift this equilibrium, the reaction conditions were systematically altered, yielding moderate improvement.[25]

To find efficient alternatives and guarantee that newly designed catalytic systems will meet adequately the requirements to be complied with the production of renewable chemicals, recent focus has shifted towards the development of heterogeneous base catalysts.[28,29] Among others, zeolites,[30,31] amorphous and crystalline mixed oxides,[32–34] carbon-based materials[35] and their composites[36] as well as doped counterparts[37] enabled the almost exclusively chemoselective fructose production in a recyclable manner, resulting in fructose yield of 15–30%. Pioneer works, however, demonstrated that the ratio of the undesired retro-aldol reaction markedly improved when glucose conversion was possible to be increased.[23,28] These reports shown that this phenomenon was closely attributed to the presence of the strong basic sites, at which the retro-aldol condensations could take place. On the contrary, in the absence of these strong basic sites, the glucose conversions get closer to the level of enzyme catalysed reactions. Therefore, it seems to be obvious that the application of catalyst with tuneable basic features would be the answer.

For that reason, layered double hydroxides (LDHs), one family of the most promising solid bases with two-dimensional, ion-intercalated, anisotropic layered structure have attracted significant interest.[38–41] These anionic clays consist of octahedrally coordinated metal hydroxide layers in which the bivalent cations are partially substituted by trivalent cations, generally.[42,43] As a result of the isomorphous substitution, the hydroxide layers are positively charged which is compensated by the interlamellar, solvated anions.[44,45] Because of their basic sites with different bonding structures and base strengths, hydrotalcites (Mg_XAl–LDHs) proved to be useful promoters for particularly high fructose-selective glucose-to-fructose reaction that even yielded considerable amount of fructose (25–56% yield).[46–56] Moreover, the application of these catalysts seemed to be more favourable from an industrial point of view than any other solid catalysts considering their long-term stability, durability as well as ability for catalysing recyclable, rapid isomerizations under variable reaction conditions.[46] Both numerous morphological and structural aspects of these bases in relation to the fructose yield could be revealed under aqueous conditions with the key contributions by Palkovits,[46,51,54] Shang[56] and Jung.[50,52,53,55] It can be concluded that in determining the total number of strong and weak basic sites, it is mainly the actual ratio of Mg(II) and Al (III) that determines the efficiency.[46] This efficiency can be changed by introducing a dehydration–rehydration process, which leads to an increase in the number of weak basic sites.[53] However, the accessibility of the basic sites depends strongly on the particle size of LDH, so that the glucose conversion/fructose yield increases with decreasing particle size.[56] On the other hand, the hydrophilicity of hydrotalcites increases in parallel with the decrease in particle size, which inhibits the sorption of glucose at the active sites and thus prevents efficient isomerization. Therefore, the particle size of the LDH catalyst has been shown to be the most important aspect affecting isomerization besides the distribution of the basic sites.

Although notable progress has been realized, no comprehensive studies can be found as yet reporting on the role of the interlamellar anions of the prepared LDHs (not dehydrated ones). Moreover, the deep understanding of the catalytic processes promoted by LDHs in ethanol, one of the most promising recent advances in the field, has not yet been fully described.[47,48] Although the report by Hwang and Fukuoka was detailed in some respects and showed very competitive catalytic isomerization with fructose up to 56% yield, many essential aspects (particle size, hydration, composition, *etc.*) were neglected.

The current study aims to find the key parameters of an LDH-catalysed glucose-to-fructose isomerization in ethanol to gain exclusive fructose selectivity. It is shown that variations in the basic strength distribution of hydrotalcites (Mg_XAl-LDH) can lead to remarkable differences in their catalytic activity and selectivity for isomerizations in ethanol. The unique role of interlamellar anions, the remarkable influence of crystallinity and water content, and the key role of the hydrophilicity of LDHs on their own catalytic behaviour and the catalytic ability of hydrocalumites (Ca_2Al-LDH) are also demonstrated.

2. Results and discussion

2.1. Catalyst characterisation

In order to focus solely on the catalytic properties of the LDHs, it seemed obvious that the disturbing effect of all undesirable structural features (phase impurities, amorphous features, defect sites, *etc.*) should necessarily be detached. For this reason, attempts were made in all cases to synthesize highly crystalline, phase-pure, carbonate-containing (in the case of Ca_2Al-LDH, nitrate-containing) layered double hydroxides (LDHs) with well-defined compositions. Using a simple co-precipitation method carried out at constant pH (pH = 10 for Mg_xAl-LDH and pH = 13.1 for Ca_2Al-LDH),[57] this goal was readily achieved. XRD analysis revealed that highly crystalline, phase-pure solid products with a rhombohedral structure were produced (Fig. 1). The XRD patterns of these rhombohedral structures were analogous to those of the corresponding inorganics, which were identified as carbonate-containing layered double hydroxides in space group 3*R* (JCPDS card: PDF#89-0460).[58] It is noteworthy that due to the variable coulombic attraction between the positively charged layers and the interlamellar anions, it can be observed that the calculated interlamellar space – calculated by using the Bragg's law (Experimental part S1†) – increased with increasing aluminium content (from 7.7 to 8.1 Å, Table 1).[59] The primary crystallite sizes calculated according to Scherrer equation (Experimental part S2†) are found in the range of 14–18 nm (Fig. 1 and Table 1), which should be considered as the medium crystallite size.[60] For hydrocalumite, a larger interlamellar gallery (8.6 Å) can be observed beside the same crystallite size (Fig. S1D and Table S1†).[61] Indeed, the increase of the interlamellar distance is due to the nitrate ions in the interlamellar region, which were inserted instead of carbonate anions for practical reasons (see in the Experimental part).[62] F–Mg_3Al-LDH, which was prepared for a comparison (it was prepared by the method used by Fukuoka *et al.*),[48] had almost the same crystallite structure as Mg_2Al-LDH (Fig. 1), however with significantly lower crystallite size (9.3 nm, Table 1). Besides, all as-prepared brucite-like structures possessed a positive surface charge (+19–41 mV, Table 1), but its magnitude clearly depended on the aluminium content.[63] Notably, the surface charge is inversely proportional to the aluminium content. Furthermore, both the specific surface area and the morphology of the LDHs are under direct control of the pH applied during the synthesis process.[64] As expected, the as-prepared hydrotalcites and hydrocalumites exhibit a regular, hexa-

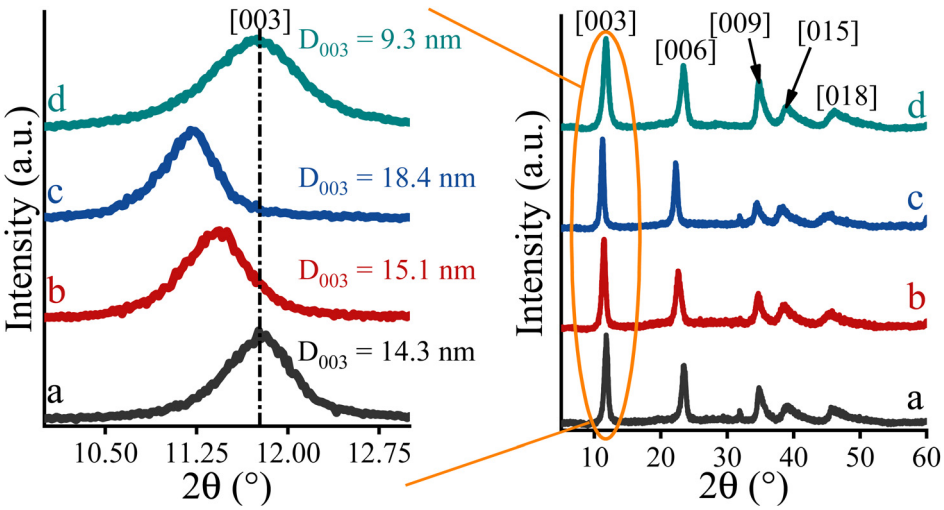

Fig. 1 XRD patterns of the as-prepared hydrotalcites (Mg_xAl-LDH): Mg_2Al-LDH (a); Mg_3Al-LDH (b), Mg_4Al-LDH (c) and F–Mg_3Al-LDH (LDH prepared by using Fukuoka's recipe[48]) (d).

Table 1 Characteristics of the as-prepared hydrotalcites

Composite	Interlamellar distance[a] (Å)	Crystallite size[b] (nm)	Actual M(II) : M(III) ratio[c]	Intrinsic basicity[d] (mmol g^{-1})	Specific surface area[e] (m^2 g^{-1})	Zeta potential[f] (mV)
Mg_2Al-LDH	7.7	14.3	1.98	0.34 ± 0.01	71	+40
Mg_3Al-LDH	8.0	15.1	3.01	0.49 ± 0.06	64	+29
Mg_4Al-LDH	8.1	18.4	3.99	0.60 ± 0.03	56	+19
F–Mg_3Al-LDH	*7.7*	*9.3*	*1.80*	*0.29 ± 0.02*	*132*	*+38*

[a] *d*(003), calculated by using the Bragg's law. [b] *D*(003), calculated by using the Scherrer equation. [c] Determined by ICP-MS. [d] Determined by non-aqueous acid–base titration. [e] Determined by N_2 sorption (BET). [f] Determined by DLS measurements. Last row: LDH prepared by using Fukuoka's recipe.[48]

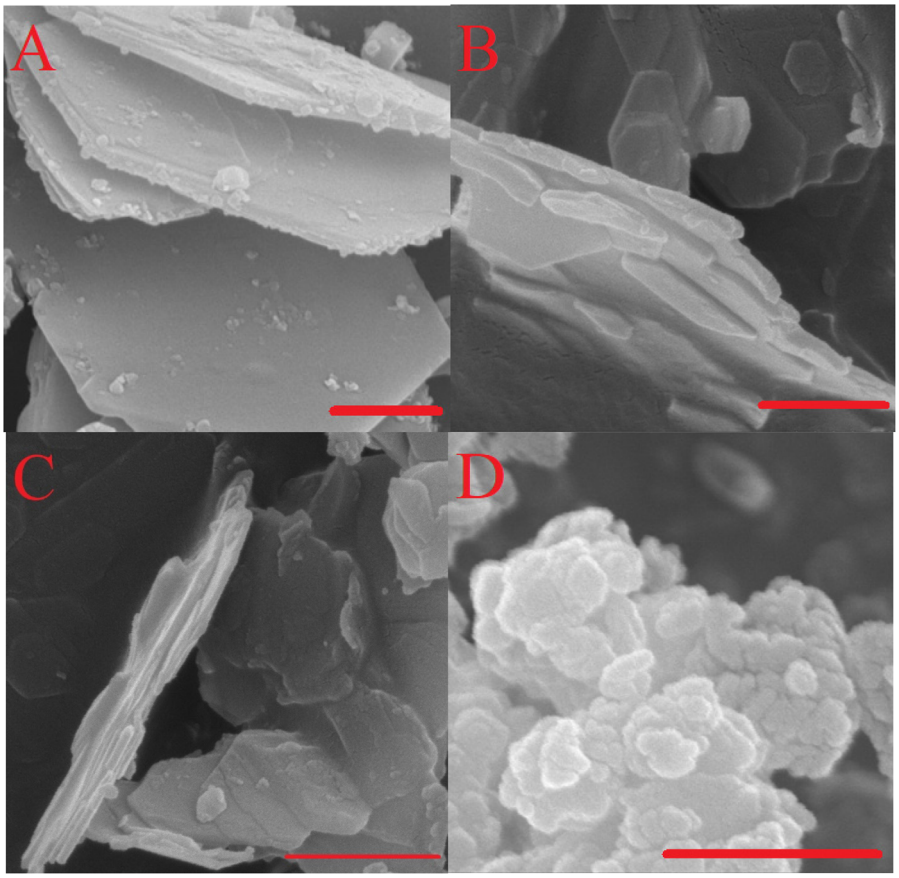

Fig. 2 SEM micrographs of the as-prepared hydrotalcites. Mg_2Al-LDH (A), Mg_3Al-LDH (B), Mg_4Al-LDH (C) and F–Mg_3Al-LDH (D). Scale bars represent 500 nm.

gonally shaped morphology (Fig. 2A–C) and a relatively low specific surface area due to the non-porous lamellar structure (Table 1 and Fig. S2†). Furthermore, by introducing ICP-MS measurements, it was possible to verify the actual M(II) : M(III) ratios, which technically matched the nominal ratios (Table 1). On the contrary, F–Mg_3Al-LDH differs greatly from others. Non-defined, grain-like morphology (Fig. 2D) and, as a result, almost two times higher specific surface area (132 $m^2\ g^{-1}$; Table 1) can be associated with this structure. Interestingly, the measured actual Mg-to-Al ratio (Table 1) showed that using this synthesis procedure, as opposed to the nominal ratio of 3 : 1, an LDH structure with an Mg-to-Al ratio of 1.8 : 1 can be produced, which is in good agreement with the results of Lee and co-workers.[65] However, this fact also clearly pinpoints that the previously published results with regard to the activity–composition relationship of hydrotalcites in the glucose-to-fructose reaction in ethanol should definitely be revised.

In order to optimize the surface parameters of LDHs to promote the efficiency of isomerization, it was necessary to carry out dehydration and dehydration/rehydration (reconstruction) processes.[66] After heat treatment, the characteristic Bragg reflections of the LDH derivatives with shifted 00*l* reflections could be identified on the XRD patterns of the partially dehydrated samples (135, 200 °C, Fig. 3, S3 and S4,† Tables 2, S2 and S3†). This shift showed that in both cases some of the interlamellar water content was released, resulting in a reduction of the interlayer space. At higher temperatures, the collapse of the long-range ordered layer structure can be observed in parallel to the formation of a mixed oxide phase (PDF#75-1525; Fig. 3d and e). However, these mixed oxide phases can be converted to LDH-s *via* rehydration. As a result, the original layered structure can be almost fully restored, but with larger interlayer distances due to the variable water and hydroxyl contents (Fig. 3f). Throughout the process, the morphology and specific surface area also changed with the change in water content. On one hand, the mixed oxides had a spherical, non-defined morphology (Fig. 3e (SEM micrographs)) in contrast to the hexagonally shaped morphology of the LDH-like structures (Fig. 3f (SEM micrographs)). On the other hand, the oxide phase had the largest specific surface areas, the exact values of which were in the range of 315–370 $m^2\ g^{-1}$ (Tables 2, S2 and S3†).

When interlamellar anions other than carbonate ions were intercalated, there were no significant differences in the texture of the solids, apart from variations in the interlamellar region (Fig. S1 and Tables S1, S4†). In particular, when nitrate ions were introduced into the interlamellar space, the interlamellar gallery expanded in all cases, as expected based on the

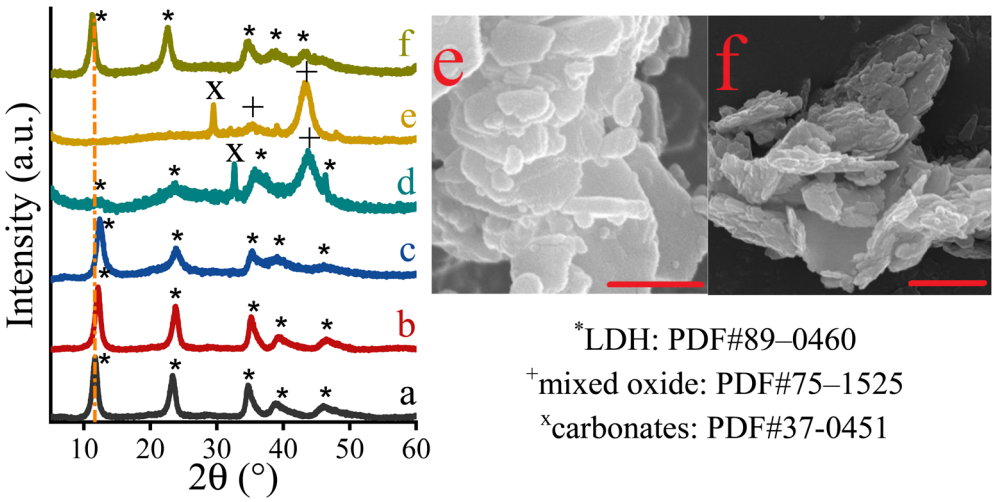

Fig. 3 XRD patterns of the heat-treated as well as rehydrated Mg_2Al-LDH: as-prepared (25 °C) (a); dehydrated at 135 °C (b); dehydrated at 200 °C (c); dehydrated at 330 °C (d); calcined at 500 °C (e) as well as calcined-rehydrated (f). SEM micrographs of the calcined (e) and calcined-rehydrated (f) LDHs. JCPDS cards of the identified phases can be seen. Scale bars represent 500 nm.

Table 2 Characteristics of the heat-treated and rehydrated Mg_2Al-LDH

Heat treatment (°C)	Interlamellar distance[a] (Å)	Crystallite size[b] (nm)	Actual M(II) : M(III) ratio[c]	Intrinsic basicity[d] (mmol g^{-1})	Specific surface area[e] (m^2 g^{-1})
135	7.6	13.9	—	0.36	—
200	7.5	13.1	—	0.41	101
330	7.5	4.2 (5.8[f])	—	0.53	175
500	—	7.8	1.98	0.61	320
500 (rehydrated)	7.7	14.1	1.97	0.48	172

[a] d(003), calculated by Bragg's law. [b] D(003), calculated by Scherrer equation. [c] Determined by ICP-MS. [d] Determined by non-aqueous acid–base titration. [e] Determined by N_2 sorption (BET). [f] Mixed oxide.

literature.[67] In addition, the 004 reflection of hydrocalumite containing chloride as charge-balancing anions doubled due to slight variations in the hydration of the different double hydroxide layers. This is a well-known phenomenon for chloride-containing hydrocalumites.[57]

Concerning the basicity of the structures of the LDH-derivatives, it can be stated that each structure has a measurable basicity, the extent of which depends on both the actual cationic ratios and the hydration of the structures (Fig. 4 and S5†). The as-prepared structures had both weak and strong basic sites (Fig. 4A).[68] It is also clear that all the structures have a higher proportion of strong basic sites than weak ones. Furthermore, the proportion of strong basic sites increased further when the dehydration treatment was applied (Fig. 4B and S5†). Moreover, the highest overall basicity is associated with the mixed oxide phases, which, however, have the highest proportion of strong basic sites (Fig. 4B).[68] During the rehydration process, the proportion of strong basic sites decreased significantly. In addition, in all cases, medium basic sites also appeared on the surfaces (Fig. 4B). Systematically changing the M(II) : M(III) ratio in the case of hydrotalcites, one can see that the trends also change with hydration (Fig. 4C). While a clear sequence Mg_2Al-LDH < Mg_3Al-LDH < Mg_4Al-LDH can be seen for the as-prepared hydrotalcites and the dehydrated (calcined) hydrotalcites, exactly the opposite order can be observed for the dehydrated/rehydrated samples.[69] In the latter case, the appearance of the excess hydroxide ions caused the formation of coordinatively unsaturated anions on the surface, whose polarizability affects their basicity.[70] Thus, the basicity of the coordinatively unsaturated anions is at maximum on the most positively charged LDH surface (Mg_2Al-LDH). To confirm our findings, a CO_2-TPD study was performed on calcined LDHs (Fig. S6 and Table S5†). This demonstrated that the trends determined by CO_2-TPD were consistent with those observed by titrations. Although the TPD measurement is more accurate one than titration it cannot be used for hydrated, carbonate-containing samples because adsorbed and "structural" carbonates cannot be distinguished by commercial TPD methods.[49] Furthermore, it was observed that the basicity of the LDH structures has a measurable dependence on the quality of the charge-balancing anions (Fig. 4D). The observed order of the contribution of interlamellar anions to the overall basicity (CO_3^{2-} > NO_3^- > Cl^-) showed good agreement with previously determined results.[68,71] Taking into account this sequence, it was expected that carbonate-containing LDHs should be superior to other hydrotalcites. Finally, it can be concluded

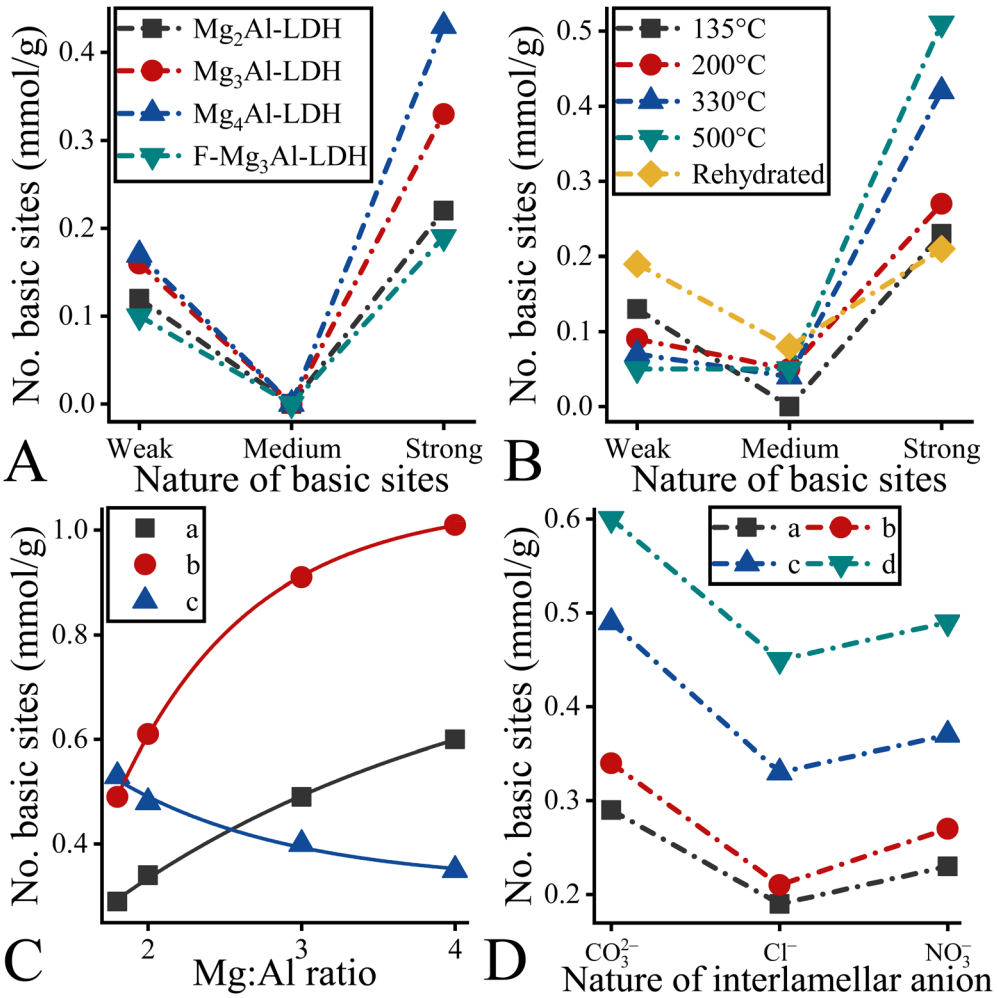

Fig. 4 Plot of the total number of basic sites for (A) as-prepared hydrotalcites, (B) heat-treated and rehydrated Mg_2Al-LDH. Total number of basic sites of as-prepared (a), calcined (b) and calcined-rehydrated (c) hydrotalcites as a function of the actual Mg(II) : Al(III) ratio of the structures (C) and (D) hydrotalcites (F–Mg_3Al-LDH (a); Mg_2Al-LDH (b), Mg_3Al-LDH (c) and Mg_4Al-LDH (d)) intercalated with different charge-compensating anions. (Lines are just to guide the eye.)

that hydrocalumites possess a higher intrinsic basicity relative to their corresponding hydrotalcite counterparts (Fig. S7 and Table S1†). However, this excess is closely related to the over-represented strong basic sites.[72]

2.2. Hydrotalcite catalysed glucose-to-fructose reaction – the role of the basic strength

Since the number of basic sites and their distribution can determine the efficiency of thermal catalytic glucose-to-fructose isomerization, the influence of the composition of LDHs on catalytic performance was first investigated (Fig. 5).[46] Both glucose conversions and fructose selectivities were found to depend on the actual molar ratios of the building block cations. When the aluminium content in the hydrotalcites was reduced, both markers decreased monotonically, which is in a good agreement with Fukuoka's results obtained under similar reaction conditions.[48] However, they identified LDH with a Mg-to-Al ratio of 3 : 1 as the most efficient candidate capable of heterogeneously promoting the isomerization of glucose to fructose. In contrast, in our study, Mg_2Al-LDH proved to be the most efficient which is in apparent contradiction to the previous results. Indeed, the synthesis method used in the Fukuoka's study allowed LDH structures to be synthesized with Mg-to-Al ratios different from the theoretical ones. In particular, when a nominal Mg-to-Al ratio of 3 : 1 was set, an LDH with an actual cationic molar ratio of 1.82 : 1 was precipitated, as presented by Lee and co-workers (this study was cited in Fukuoka's paper).[65] This was also confirmed by our ICP-MS measurement of the F–Mg_3Al LDH (1.8 : 1 Mg-to-Al ratio, Table 1). In spite of the similar structure and composition, the most efficient one of our as-prepared LDHs (that is the Mg_2Al-LDH) gives a higher overall fructose yield than that was observed by Fukuoka under similar conditions (Table 3). The reasons for this probably lie in the striking differences in the morphology of the catalysts mentioned above (Fig. 2). This will be discussed detail in section 2.4.

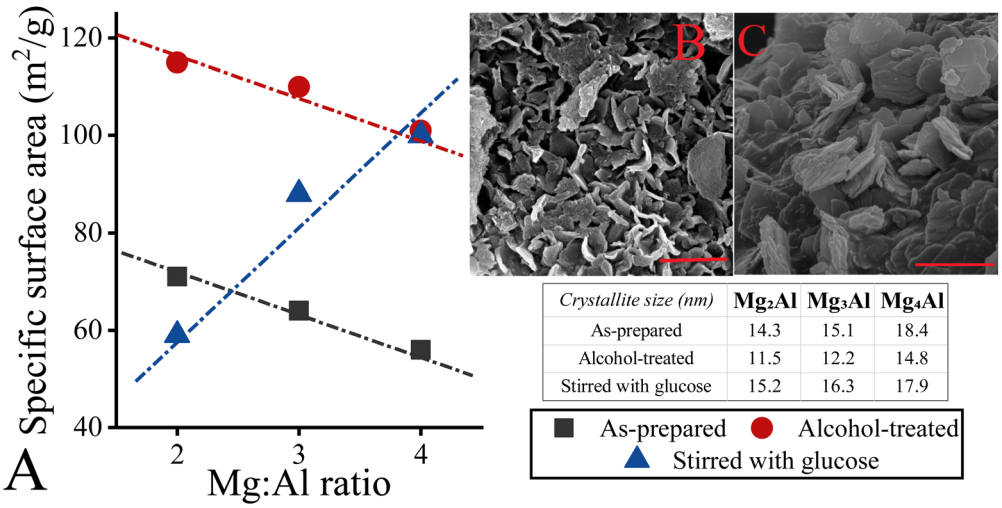

Fig. 5 Specific surface area of the as-prepared (black squares), alcohol-treated (wine-coloured circles) and glucose-treated hydrotalcites as a function of the actual Mg(II) : Al(III) ratio of the structures (A). SEM micrographs of alcohol-treated (B) and glucose-treated (C) Mg_2Al-LDH. Scale bars represent 500 nm. Crystallite size of the solids obtained can also be seen in the figure that sizes were calculated by Scherer equation ($D(003)$). (The dash-dotted lines are just a guide to the eye.)

Table 3 Results of catalytic test reactions of carbonate-containing hydrotalcites. Reaction conditions: glucose (100 mg), ethanol (14 mL), catalyst (100 mg), T = 80 °C, t = 2 h

Composites	Glucose conversion (mol%)	Fructose selectivity[a] (mol%)	Fructose yield[b] (mol%)	Intrinsic basicity[c] (mmol g^{-1})
Mg_2Al-LDH	64 ± 3	82	53 ± 5	0.34 ± 0.01
Mg_3Al-LDH	53 ± 2	76	40 ± 2	0.49 ± 0.06
Mg_4Al-LDH	45 ± 2	73	33 ± 3	0.60 ± 0.03
F–Mg_3Al-LDH	*54 ± 3*	*78*	*42 ± 4*	*0.29 ± 0.02*

[a] Glucose conversion/fructose yield) × 100%. [b] NMR yield. [c] Determined by acid–base titration. ITALIC: catalyst prepared by Fukuoka's recipe.

These results are indeed very surprising. As described in detail above, the acid–base titrations give a clear sequence of LDHs with different aluminium content in terms of basicity, with the basicity of the LDHs increasing with decreasing aluminium content. In other words, Mg_2Al-LDH should be the less active catalyst in this reaction as it has the least number of basic sites. This observation should be taken as an indication that the change in other properties of LDHs determines the catalytic performance in alcohols. It is to be mentioned here that our results related to the basicity of the LDHs cannot be directly compared with the results of Fukuoka, as their results were related to non-phase-pure products and the presence of surface aluminium-pure phases may obscure the actual basic character of the LDH surfaces. The evaluation of the NMR data also showed that mannose and acetic acid were produced as by-products in detectable quantities. This is in a good agreement with the results of Marianou *et al.* who found similar selectivities of this reaction in non-aqueous solutions however using MgO heterogeneous catalyst.[73]

2.3. Hydrotalcite catalysed glucose-to-fructose isomerization – the role of the hydrophilicity

Palkovits and co-workers have shown that LDH has a ratio of 0.23 < Al/(Mg + Al) < 0.30 to work efficiently, which corresponds to an actual Mg-to-Al ratio of ~3 : 1.[46] However, they also made it clear that when isomerization is carried out – noticeably in water –, there is no clear relationship between the catalytic efficiency and the molar ratio of the cations when freshly prepared LDH specimens are used.[46] In this case, the accessibility of the active sites was crucial for the efficiency. Therefore, changing the crystallite size and specific surface area can lead to significant differences. So, the focus of this study at this point was shifted to determining the agglomeration characteristics of LDHs in order to understand the crucial influence on catalytic efficiency. However, there were no significant differences found either in the specific surface areas (10–19 $m^2\ g^{-1}$ or 105–115 $m^2\ g^{-1}$, Fig. 5A, Table S6†) or in the crystallite sizes (14–18 or 10–13 nm, Fig. 5, Table S6†) when the LDHs were examined after the synthesis procedure or after ethanolic treatment, which was performed to rule out the occurrence of an AMO (Aqueous Miscible Organic)-like effect.[74] Remarkably, the specific surface area of all treated LDHs changed as a result of the ethanolic treatment, but the effect was the same for all hydrotalcites and their surface areas did not differ significantly from each other. This expansion can be closely related to the changes in the morphology (Fig. 5B), allowing rose-like morphology with well-ordered hydroxide layers.

When the alcoholic treatment was repeated in the presence of glucose at 40 °C, remarkable changes were observed. The specific surface areas decreased to a maximum at the aluminium content of the LDHs (Fig. 5A): Mg_4Al-LDH (107 $m^2\ g^{-1}$) > Mg_3Al-LDH (88 $m^2\ g^{-1}$) > Mg_2Al-LDH: (59 $m^2\ g^{-1}$). This

is probably due to the differences in glucose sorption capacity of the as-prepared hydrotalcites. In particular, when a large number of glucose can be adsorbed on the surface of LDH, a higher degree of aggregation of the LDH particles can be hypothesized due to the surface charge neutralization associated with the partial or complete deprotonation of glucose.[47] This hypothesis is also strengthened by the SEM micrograph of "glucose-treated" LDHs, exhibiting solid structures with aggregated lamellae (Fig. 5C). To test our hypothesis, we performed both time-dependent DLS measurements and adsorption experiments. For theoretical reasons, it was possible to use a maximum glucose concentration of 7.5 mg L^{-1} and a LDH concentration of 7.5 mg L^{-1} for the DLS measurements.[75,76] Nevertheless, the final mass ratio of glucose-to-LDH was the same as for the catalytic reactions. The aggregation of the different hydrotalcites is varied, but this cannot be related to the initial differences in surface charge. In particular, in the presence of glucose, the LDH with the highest surface charge (Mg_2Al-LDH; + 40 mV) can aggregate more readily (Fig. 6A) than others (Fig. 6B and C). This was especially the case when the glucose-to-LDH mass ratio was the same as in the catalytic tests. Moreover, the sorption experiments showed that Mg_2Al-LDH took up a much larger amount of glucose compared to Mg_3Al-LDH and Mg_4Al-LDH (Fig. 6C). The obtained trends and curves can be readily described using the Langmuir model,[77] which can also be used to determine the sorption capacity. On this basis, Mg_2Al-LDH (739 mg g^{-1}) has twice the glucose sorption capacity of that of Mg_4Al-LDH (342 mg g^{-1}) and a 1.5-fold higher capacity compared to the Mg_3Al-LDH system (501 mg g^{-1}). It can therefore be excluded that the zeta potentials (surface charges) alone determine the catalytic efficiency. The other important property that has a significant influence on the sorption capacity, especially in this case, is the hydrophilicity of the LDH surfaces.[78] It has already been established that the surface basicity and hydrophilicity of hydrotalcites are almost linearly proportional.[79] Considering that the basicity of hydrotalcites decreases in the order Mg_4Al-LDH > Mg_3Al-LDH >

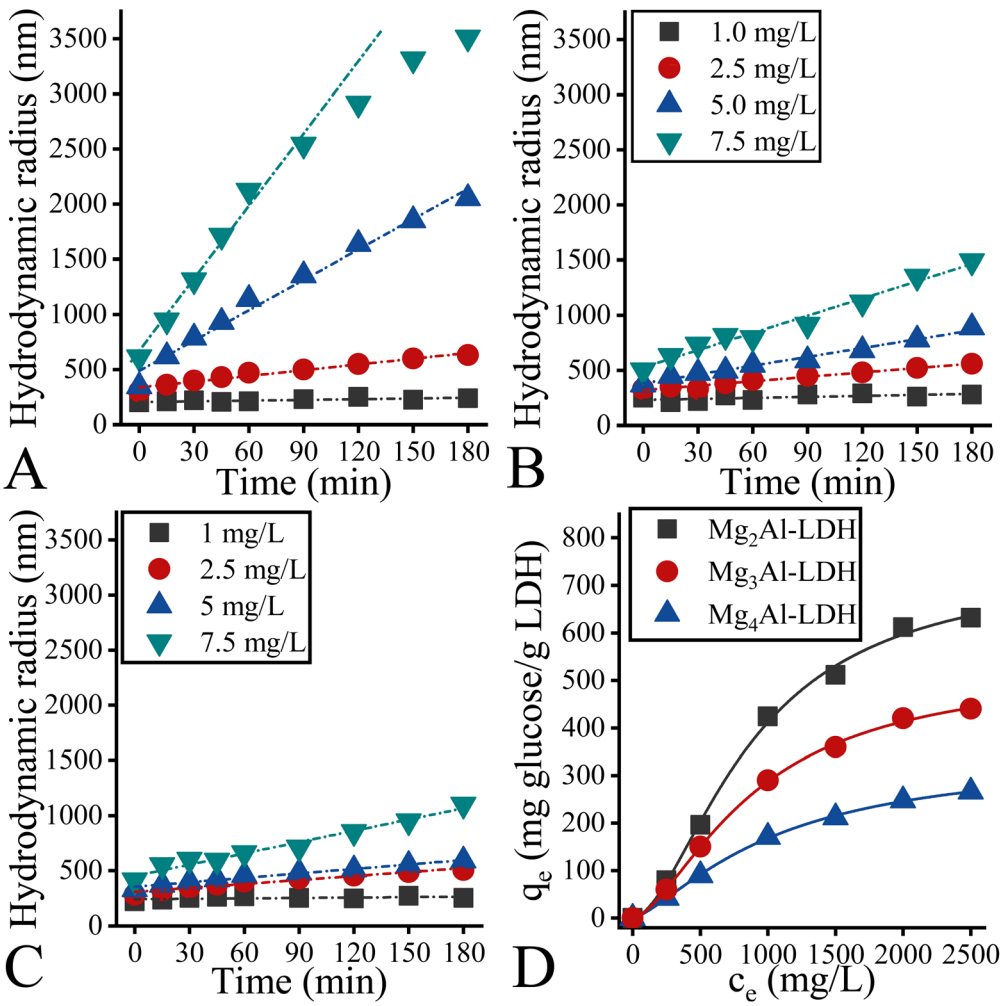

Fig. 6 Hydrodynamic radii of Mg_2Al-LDH (A), Mg_3Al-LDH (B) and Mg_4Al-LDH (C) (5 mg L^{-1}) as a function of time of the experiment measured at different glucose concentrations. Glucose adsorption isotherm (D) of different hydrotalcites (100 mg L^{-1}). The solid lines are fits using the Langmuir model.

Mg_2Al-LDH, it seems clear that Mg_2Al-LDH is the most hydrophobic compared to the other hydrotalcites tested. This assumption agrees well with the results of the DLS and sorption experiments, because glucose can be adsorbed quite reliably on more hydrophobic (Mg_2Al-LDH) than on hydrophilic surfaces (Mg_3Al-LDH; Mg_4Al-LDH). Indeed, the adsorption of glucose molecules is more strongly influenced by hydrophobic interactions than by hydrophilic ones, as Fukuoka and co-workers have already found.[80] Although the remarkable role of the hydrophilicity of LDH has been highlighted before (in aqueous solutions), it proved to be the crucial feature of the LDH catalyst to work efficiently in the isomerization of glucose to fructose in alcoholic solutions.

2.4. Hydrotalcite catalysed glucose-to-fructose isomerization – the role of the water-content

In Fukuoka's work, it was really surprising that the catalytic markers did not increase when a reconstitution process (dehydration/rehydration) was introduced to avoid deactivation of the LDH surface.[48] In aqueous systems, the principle is that activated LDHs are more useful than fresh ones because their basic strength distribution changes during the reconstitution process, which was also established by our acid–base titrations (Fig. 4 and S5†). This also highlights the fact that the hydrophilic properties are probably more important in this system than in aqueous media. In order to vary the hydrophilicity–basicity relationship associated with the LDH structures, heat treatment was performed at 4 different reaction temperatures (135, 200, 330 and 500 °C).[55,79] In addition, rehydration of the calcined (500 °C) systems was also attempted. When isomerizations were performed with the thus treated samples (Fig. 7 and S8†), the catalytic performance changed significantly and the efficiency began to be driven by intrinsic basicity in parallel with the decrease in the water content of the LDHs. While the conversions started to decrease when the treatment temperature of 135 °C was applied, the selectivities remained unchanged compared to the hydrated samples. The partially dehydrated samples were found to be significantly less active overall than their fully hydrated counterparts. On this basis, it must be assumed that the water content adsorbed on the surface contributes significantly to the glucose conversions. Otherwise, glucose conversions should not decrease because the structural integrity of LDH and the distribution of base sites are not affected. With continued dehydration (200 °C), the observed decrease in glucose conversion was found to enhance compared to the last condition, while the selectivity data did not vary with changes in hydration of LDHs. This suggests that fructose selectivity is under the control of the weak basic sites, the value of which did not change with dehydration/calcination (Fig. 4). On the contrary, the extent of glucose conversion can be related to the efficiency of adsorption, which thus indirectly depends on the hydrophilicity of the surface of the LDH derivative. Therefore, the increased intrinsic basicity of the dehydrated samples exerted a negative impact on the catalytic performance. These trends continued in parallel with the increase in temperature of the heat treatment. The mixed oxide phase (500 °C) showed the worst catalytic performance.

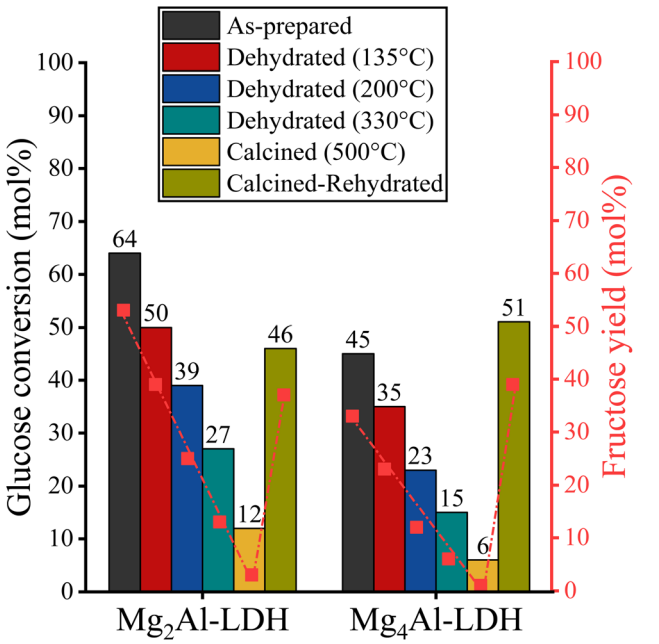

Fig. 7 Catalytic performances of the as-prepared and treated Mg_2Al-LDH and Mg_4Al-LDH. Reaction conditions: glucose (100 mg), ethanol (14 mL), catalyst (100 mg), T = 80 °C, t = 2 h. Squares indicate fructose yield. (The dash-dotted lines are just a guide to the eye.)

Recognizing the major role of hydrophilicity and water adsorbed on the surface in this transformation, an attempt was made to determine the effects of dehydration/rehydration of hydrotalcites on the catalytic ability of LDHs. Although catalytic isomerizations were also carried out over reconstructed structures (Fig. 7), the desired product was obtained with a reduced level of catalytic markers, particularly in glucose conversion compared to the performance of the freshly prepared samples. Moreover, the evolution of the reaction markers did not follow the trend of intrinsic basicity, which was reversed for the freshly prepared samples (Mg_2Al-LDH > Mg_3Al-LDH > Mg_4Al-LDH), in agreement with data published in the literature.[48,69] This result underlines that the catalytic performance of hydrated (fresh or reconstituted) LDHs is controlled by hydrophilicity and not by intrinsic basicity.

Moreover, these results with reconstructed samples have lagged behind those previously published.[47,48] This observation is probably due to the morphological aspects of the catalysts. While the Fukuoka's catalyst had a non-defined, grain-like morphology with relatively small crystallite size (~10 nm) and accessible outer sites, our reconstructed samples had a well-defined, plate-like morphology that allows the basic sites on the inner surface to be available to a greater extent than other morphologies. This made the OH groups with strong basicity, which are enriched on the outer surface after the reconstruction procedure and are accessible, shifting the reaction towards saccharide degradation.

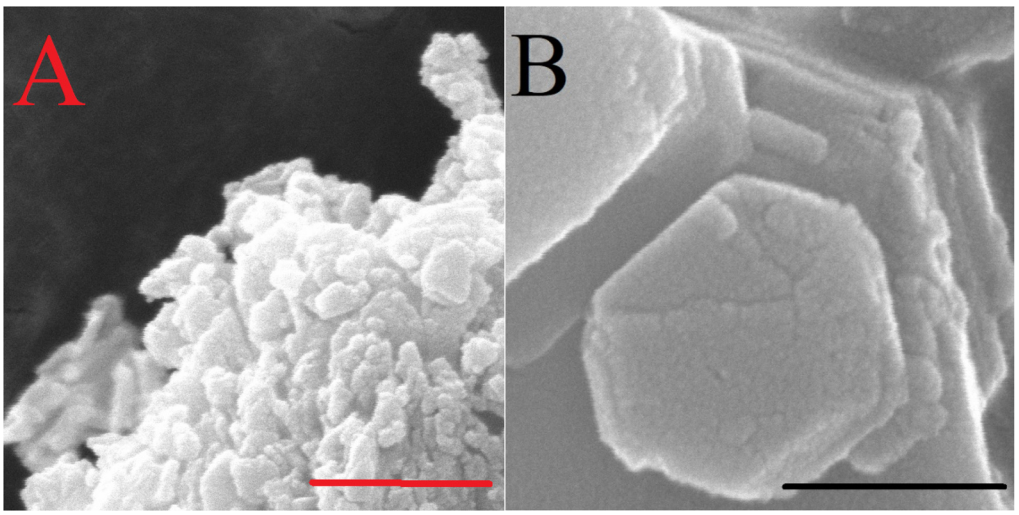

Fig. 8 SEM micrographs of calcined rehydrated F–Mg_3Al-LDH (A) and Mg_2Al-LDH (B). Scale bars represent 500 nm.

Compared to the freshly prepared Fukuoka's samples, this morphological aspect probably also leads to significant changes in the catalytic performance of our structures (Fig. 8).

Table 4 Characteristics and catalytic performance of the as-prepared, hydrothermal-treated and hot aged Mg_2Al-LDH. Reaction conditions: glucose (100 mg), ethanol (14 mL), catalyst (100 mg), T = 80 °C, t = 2 h

Characteristics	Non-treated	Hydrothermal-treated	Hot aged
Crystallite size (nm)[a]	14.3	9.9	28.0
Specific surface area ($m^2\ g^{-1}$)[b]	71	172	30
Glucose conversion (mol%)	64	49	62
Fructose yield (mol%)[c]	53	38	37
Fructose selectivity (%)[d]	82	77	60

[a] Determined by Scherrer equation. [b] Determined by N_2 sorption (BET). [c] NMR yield. [d] Glucose conversion/fructose yield) × 100%.

Indeed, LDHs with a smaller crystallite size (7–9 nm) were found to be more hydrophilic than those with medium-size crystallites (14–20 nm). Accordingly, the latter can perform well in our hydrophilicity-sensitive system, in contrast to the basic-controlled systems in aqueous media. To illustrate how morphology dictates the catalytic efficiency, post-synthetic treatments on our as-prepared Mg_2Al-LDH were performed (Table 4 and Fig. 9).[81,82] While hydrothermal-treatment caused a significant decrease in crystallite size,[81] hot ageing resulted in a significant growth in crystallite size.[82] These changes are also reflected in the morphologies. In the first case, a grain-like morphology evolved, while in the second case, a stone-like morphology was observed. Furthermore, the catalytic markers also change with the change in hydrotalcite catalyst morphology. On one hand, the decreased glucose conversion produced by the hydrothermally treated LDH is probably due to the more hydrophilic surface, similar to the effect observed by

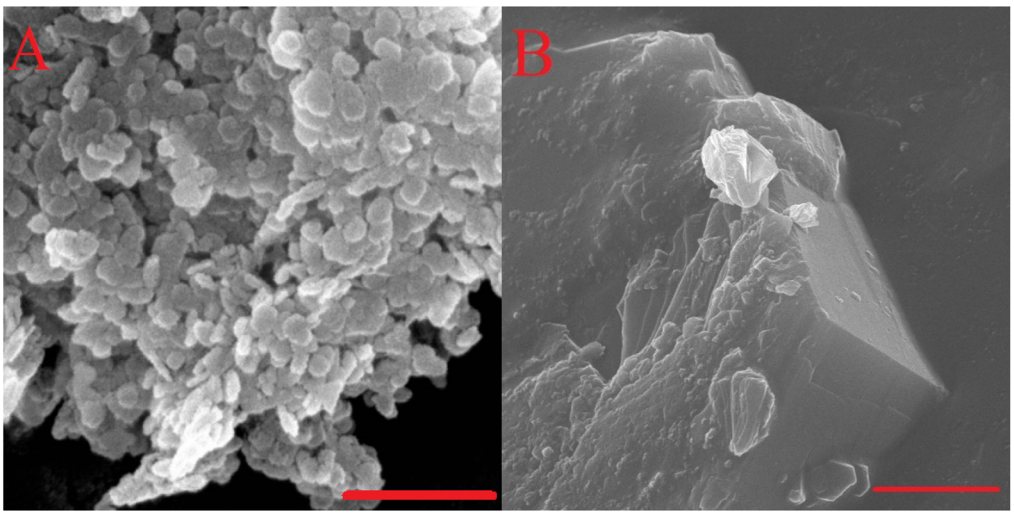

Fig. 9 SEM micrographs of hydrothermally treated (A) and hot aged (B) Mg_2Al-LDH. Scale bars represent 500 nm.

Shang *et al.* in aqueous media.[56] On the other hand, with the stone-like morphology of the LDH, access to the internal centres can be excluded in the case of the hot-aged sample.[83] Thus, the basic sites at the edge positions with strongly basic features determine the progress in catalytic performance, which, however, also enables the performance of sugar degradation and reduces fructose selectivity.

2.5. Hydrotalcite catalysed glucose-to-fructose isomerization – the role of the charge-balancing anions

Since the accessibility of the basic sites and the hydrophilicity of the LDH structure play a decisive role in this catalytic system, it has been arisen that both parameters can be readily altered by changing the charge-balancing anions (Fig. 10). Nevertheless, there is no study on the role of anionic components in freshly prepared LDHs for isomerizations. For those reasons, LDHs containing carbonate, nitrate and chloride were selected for the tests. A clear trend emerged when catalytic isomerizations were carried out. Carbonate- and nitrate-containing systems achieved higher glucose conversions and overall higher fructose yield, but the chloride-containing systems showed almost exclusively fructose selectivity. It can be readily explained by considering the followings. Base strength in freshly prepared LDH can be increased by replacing the weak basic interlamellar anion such as chloride with a stronger base such as nitrate or carbonate.[84] Increasing the base strength increases glucose conversion, but this is what makes the above-mentioned side reaction, retro-aldol condensation, favourable to isomerization. When chloride-containing LDHs are used, the absence of the strong basic sites can almost completely lead to fructose-selective isomerisation.[48,84]

Interestingly, the nitrate-containing system proved to be the most efficient catalyst, offering a glucose conversion of 71% with a fructose selectivity of 83% (fructose yield: 59%). This is probably related to the better accessibility of the internal basic sites due to the relatively large interlamellar distance in the nitrate-containing system (9.0 Å *versus* 7.7 Å (carbonate, chloride)).[67] This finding supported Fukuoka's statement that the inner sphere might play a role in isomerization in contrast to other organic reactions.[48] The catalytic performance of NO_3–Mg_2Al-LDH is comparable to the efficiency of the homogeneous and heterogeneous catalysts used as references (Table S7†), regardless of whether they are used in aqueous or in alcoholic media. Moreover, it should be noted here that the nitrate-containing system works well without requiring a high reaction temperature (above the boiling point) with autogenous or even higher pressure to shift the equilibrium. The time-dependent study on the nitrate-containing catalyst showed that both fructose yield and glucose conversion increased monotonically in the first regime of the conversion/yield-time curve (Fig. 11). This range extended from 0 to 60 minutes and after this range the markers became constant. In other words, 60 minutes is sufficient time for this system to reach maximum fructose yield. From the linear regime of the

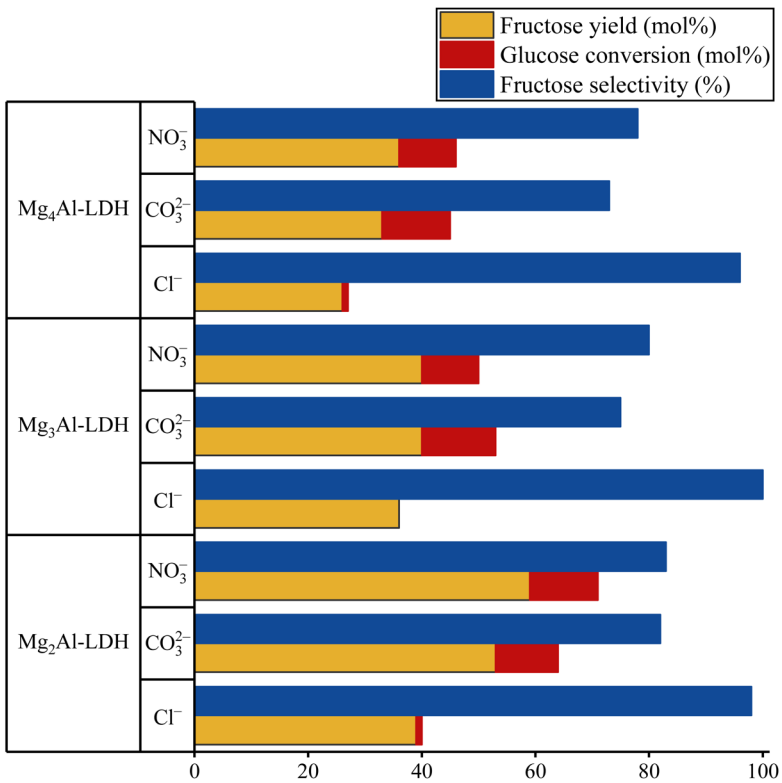

Fig. 10 Catalytic performance of the hydrotalcites loaded with different charge-compensating anions. Reaction conditions: glucose (100 mg), ethanol (14 mL), catalyst (100 mg), T = 80 °C, t = 2 h.

fructose conversion-reaction time curve, the TOF value could be calculated. This value was lower than that previously described for the LDH catalyst.[48] However, this is a clear consequence of the more accessible basic sites, which are very conducive to reach the goal of selective fructose production.

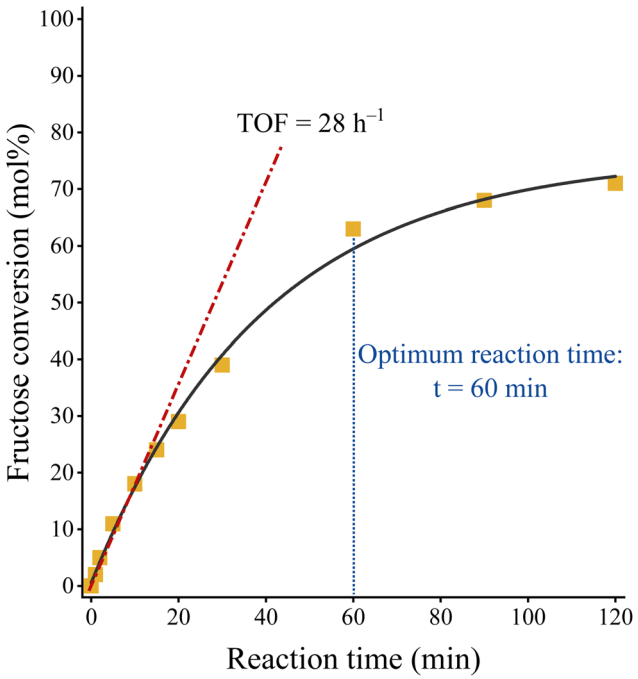

Fig. 11 Fructose conversion as a function of time of a NO_3–Mg_2Al-LDH catalysed glucose-to-fructose isomerization reaction. Reaction conditions: glucose (100 mg), ethanol (14 mL), catalyst (100 mg), T = 80 °C. TOF was calculated form the initial isomerization rate marked with wine-coloured dash-dot line considering the amounts of basic sites of the catalyst (Fig. 4).

2.6. Recyclability and heterogeneous feature of the NO_3–Mg_2Al catalyst

In order to demonstrate the heterogeneous and recyclable properties of the as-prepared catalyst, both hot filtration tests (Fig. 12A) and recycling tests (Fig. 12B) were carried out. During the hot filtration test, glucose conversion did not increase after the solid LDH was filtered from the alcoholic solution. The test thus confirmed that no catalytically active LDH specimen leached into the ethanolic phase. The final solution obtained was measured with ICP-MS and no leached cations could be detected in it. This is an advance of this method compared to the aqueous systems where significant magnesium leaching was detected. When the recycling tests were carried out, the catalytic performance of the as-prepared LDH was found to be stable for up to 3 cycles, apart from a slight variation in selectivity. This also means that the accumulation of humic acids on the surface of the catalysts did not occur as it did earlier when hydrotalcites were used as catalysts in ethanol. This is probably related to the lower reaction temperature at which our catalyst can work effectively, unlike the previous ones. Indeed, the higher reaction temperature (and pressure) favours the production of humic acids. These results indicate that the as-prepared nitrate-containing Mg_2Al-LDH system can be used as an active, selective and heterogeneous catalyst for the glucose-to-fructose isomerization in ethanol.

2.7. Hydrocalumite catalysed glucose-to-fructose isomerization

Hydrocalumites were also investigated for their ability to promote this isomerization (Fig. 13). The results obtained finally confirmed the explanations given below in relation to hydrotalcites. On one hand, hydrocalumites, which have a large number of weak and strong basic sites (Fig. S7†),[72] can undoubtedly catalyse glucose conversion. On the other hand, their remarkable hydrophilicity allowed them to produce only

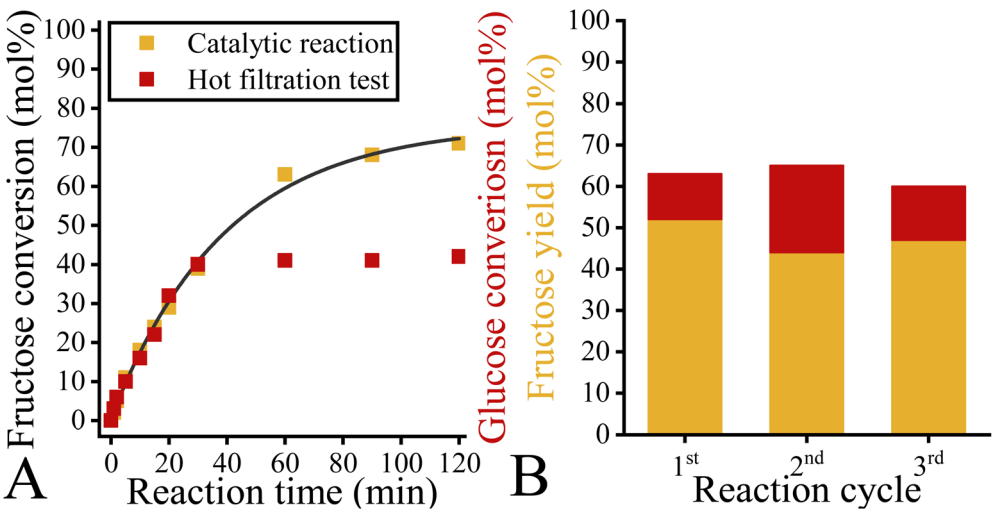

Fig. 12 Hot filtration test (A) and recycling tests (B) of the as-prepared NO_3–Mg_2Al-LDH catalyst. Reaction conditions: glucose (100 mg), ethanol (14 mL), catalyst (100 mg), T = 80 °C, t = 1 h (for recycling tests).

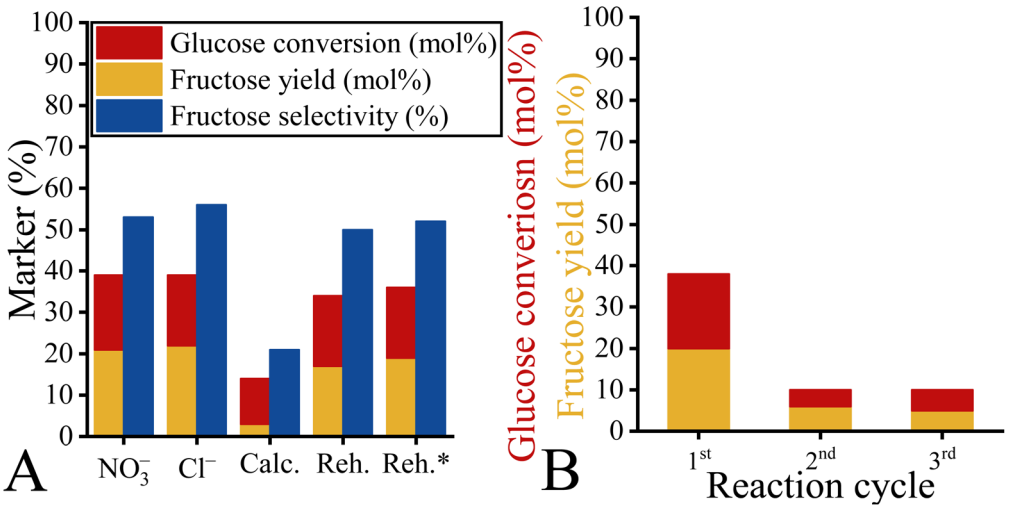

Fig. 13 Catalytic performance of hydrocalumites (NO_3^-: NO_3–CaAl-LDH; Cl^-: Cl–CaAl-LDH; Calc.: calcined hydrocalumite; Reh.: calcined-rehydrated hydrocalumite; Reh.*: carbonate-containing calcined-rehydrated hydrocalumite) (A) and recycling tests of NO_3–CaAl-LDH (B). Reaction conditions: glucose (100 mg), ethanol (14 mL), catalyst (100 mg), T = 80 °C, t = 2 h.

small amounts of fructose, which is consistent with the relationships described earlier. Furthermore, the application of dehydration or dehydration/rehydration processes showed the same trend as the hydrotalcites. Neither the mixed oxide nor the rehydrated phases can match the performance of the freshly prepared catalyst in terms of catalytic ability. It is noteworthy, however, that the catalytic behaviour of the ion-exchanged hydrocalumites is very different from that of their hydrotalcite-based counterparts. No remarkable anion dependence is observed for hydrocalumites, suggesting that in this case the relationship between basicity and hydrophilicity does not necessarily follow the trend observed for hydrotalcites. Interestingly, hydrocalumites could not be recycled because deactivation occurred in the first cycle, which prevented recycling. This is likely to be due to the collapse of the layered structure, as confirmed by XRD analysis (Fig. S9†). This may be caused by the release of calcium ions in the presence of glucose/fructose.

3. Conclusions

The most influential structural and surface properties of hydrotalcites (Mg_XAl-LDH) and hydrocalumites (Ca_2Al-LDH) have been identified, which allow the isomerization of glucose-to-fructose in ethanol to work much more efficiently than those in the works published in the literature. In contrast to the aqueous system, where activated (dehydrated/rehydrated) LDHs were found to be the most efficient promoters, the pure, as-prepared brucite-like catalysts are superior to both the heat-treated oxide/oxide-hydroxide phases and their activated counterparts. Apart from the existence of the weak and medium basic sites, which are crucial for promoting this isomerization, the surface hydrophilicity of the catalyst is the decisive factor. This can be readily modified by modifying (i) the actual molar ratio of the cations M(II) : M(III) and (ii) the crystallite size of the solids. Based on these results, it can be concluded that both the catalytic activity and the fructose selectivity of the hydrotalcites increase in the order Mg_2Al-LDH > Mg_3Al-LDH > Mg_4Al-LDH. However, this order is inversely proportional to their intrinsic basicity, because as basicity increases, so does the hydrophilicity of the LDH surfaces. For optimal performance, the crystallite size of the catalyst must be in the medium size range (14–30 nm), otherwise glucose conversion will decrease in parallel with reducing the glucose adsorption capability of the LDHs. This is due to the direct consequence of the increased surface hydrophilicity associated with the reduction in size of the LDHs. The accessibility of the basic sites also appears to be a critical factor. Since the platelet-like morphology makes the inner sphere positions more accessible compared to the grain-like morphology, the platelet-like hexagonally shaped morphology is favourable in the isomerizations. At these inner sphere positions are the charge-compensating anions, which have a remarkable influence on the actual basicity of the hydrated hydrotalcite-like catalysts. When these charge-compensating anions are systematically changed in the interlamellar region, significant differences can be observed. The efficiency of the actual catalyst changed by changing the anions in the layer in the order NO_3^- > CO_3^{2-} > Cl^-. However, chloride-containing LDH derivatives showed almost exclusive fructose selectivity, which can be readily attributed to the weaker basic character of the chloride anions facilitating isomerization. Hydrocalumite analogues behaved quite similarly to hydrotalcites, but showed lower fructose selectivity and glucose conversion due to their overly strong basic character and, as a result, enhanced hydrophilicity. These allowed undesirable retro-aldol condensation reactions however they caused lower glucose adsorption. Overall, the as-prepared nitrate-containing Mg_2Al-LDH proved to be the most efficient catalyst (71% glucose conversion, 83% fructose

selectivity, 59% fructose yield) for the isomerization of glucose-to-fructose in ethanol. This performance was established at a much lower temperature (120 °C → 80 °C) than that at which the benchmark catalysts can operate efficiently for a useful reaction time (1 hour) in an open system without the need of argon atmosphere. In addition, this catalyst appears to be recyclable and stable. Its stable feature is supported by the fact that there was no leaching of cations or accumulation of humic acids on its surface during the catalytic processes.

Conflicts of interest

There are no conflicts of interest to declare.

Acknowledgements

This work was supported by the University of Szeged Open Access Fund (Grant Number: 6407). One of us, TT Nguyen thanks for the Vingroup Science and Technology Scholarship Program for Overseas Study for Master's and Doctoral Degrees for sponsoring the opportunity to pursue her degree at UQ. The financial helps are highly appreciated.

References

1 H. Li, S. Yang, S. Saravanamurugan and A. Riisager, *ACS Catal.*, 2017, **7**, 3010–3029.
2 J. S. White, *Am. J. Clin. Nutr.*, 2008, **88**, 1716–1721.
3 X. Guo, H. Zhu, Y. Si, X. Lyu, Y. Cheng, L. Zheng, L. Wang and X. Li, *Ind. Eng. Chem. Res.*, 2022, **61**, 7216–7224.
4 C. Lin, H. Wu, J. Wang, J. Huang, F. Cao, W. Zhuang, Y. Lu, J. Chen, H. Jia and P. Ouyang, *Ind. Eng. Chem. Res.*, 2020, **59**, 4358–4366.
5 Y. Yin, C. Ma, W. Li, S. Luo, Z. Zhang and S. Liu, *ACS Sustainable Chem. Eng*, 2022, **10**, 17081–17093.
6 A. T. Hoang, A. Pandey, Z. Huang, R. Luque, K. H. Ng, A. M. Papadopoulos, W. H. Chen, S. Rajamohan, H. Hadiyanto, X. P. Nguyen and V. V. Pham, *ACS Sustainable Chem. Eng*, 2022, **10**, 3079–3115.
7 J. Ethiraj, D. Wagh and H. Manyar, *Energy Fuels*, 2022, **36**, 1189–1204.
8 Y. Román-Leshkov, C. J. Barrett, Z. Y. Liu and J. A. Dumesic, *Nature*, 2007, **447**, 982–985.
9 H. Guo, T. Dowaki, F. Shen, X. Qi and R. L. Smith, *ACS Sustainable Chem. Eng*, 2022, **10**, 9002–9021.
10 E. Lam and J. H. T. Luong, *ACS Catal.*, 2014, **4**, 3393–3410.
11 A. Corma Canos, S. Iborra and A. Velty, *Chem. Rev.*, 2007, **107**, 2411–2502.
12 S. H. Bhosale, M. B. Rao and V. V. Deshpande, *Microbiol. Rev.*, 1996, **60**, 280–300.
13 R. A. Sheldon and D. Brady, *Chem. Commun.*, 2018, **54**, 6088–6104.
14 C. Tian, J. Yang, C. Liu, P. Chen, T. Zhang, Y. Men, H. Ma, Y. Sun and Y. Ma, *Nat. Commun.*, 2022, **13**, 1–13.
15 N. Wagner, A. Bosshart, J. Failmezger, M. Bechtold and S. Panke, *Angew. Chem., Int. Ed.*, 2015, **54**, 4182–4186.
16 L. Yang, X. C. Wang, M. Dai, B. Chen, Y. Qiao, H. Deng, D. Zhang, Y. Zhang, C. M. Villas, B. de Almeida, A. S. F. Chiu, J. J. Klemeš and Y. Wang, *Energy*, 2021, **228**, 120533.
17 R. Bermejo-Deval, M. Orazov, R. Gounder, S. J. Hwang and M. E. Davis, *ACS Catal.*, 2014, **4**, 2288–2297.
18 Y. Román-Leshkov, M. Moliner, J. A. Labinger and M. E. Davis, *Angew. Chem., Int. Ed.*, 2010, **49**, 8954–8957.
19 J. C. Speck, *Adv. Carbohydr. Chem.*, 1958, **13**, 63–103.
20 S. S. Chen, D. C. W. Tsang and J. P. Tessonnier, *Appl. Catal., B*, 2020, **261**, 118126.
21 W. J. Goux, *J. Am. Chem. Soc.*, 1985, **107**, 4320–4327.
22 Q. Yang, M. Sherbahn and T. Runge, *ACS Sustainable Chem. Eng*, 2016, **4**, 3526–3534.
23 S. Zhao, X. Guo, P. Bai and L. Lv, *Asian J. Chem.*, 2014, **26**, 4537–4543.
24 J. M. Carraher, C. N. Fleitman and J. P. Tessonnier, *ACS Catal.*, 2015, **5**, 3162–3173.
25 P. Drabo, M. Fischer, M. Emondts, J. Hamm, M. Engelke, M. Simonis, L. Qi, S. L. Scott, R. Palkovits and I. Delidovich, *J. Catal.*, 2023, **418**, 13–21.
26 Q. Yang and T. Runge, *ACS Sustainable Chem. Eng*, 2016, **4**, 6951–6961.
27 C. Liu, J. M. Carraher, J. L. Swedberg, C. R. Herndon, C. N. Fleitman and J. P. Tessonnier, *ACS Catal.*, 2014, **4**, 4295–4298.
28 I. Delidovich, *Curr. Opin. Green Sustainable Chem*, 2021, **27**, 100414.
29 V. Toussaint and I. Delidovich, *Catal. Sci. Technol.*, 2022, **12**, 4118–4127.
30 I. Graça, D. Iruretagoyena and D. Chadwick, *Appl. Catal., B*, 2017, **206**, 434–443.
31 S. Saravanamurugan, M. Paniagua, J. A. Melero and A. Riisager, *J. Am. Chem. Soc.*, 2013, **135**, 5246–5249.
32 J. Ren, X. Ye, X. Shi, H. Xu, L. Wu and T. Wang, *React. Chem. Eng.*, 2022, **7**, 1786–1796.
33 D. M. Gao, Y. B. Shen, B. Zhao, Q. Liu, K. Nakanishi, J. Chen, K. Kanamori, H. Wu, Z. He, M. Zeng and H. Liu, *ACS Sustainable Chem. Eng*, 2019, **7**, 8512–8521.
34 D. C. W. Tsang, K. C. W. Wu, S. S. Chen, Y. Cao, J. P. Tessonnier, J. Shang, D. Hou, Z. Shen, S. Zhang and Y. S. Ok, *ACS Sustainable Chem. Eng*, 2020, **8**, 6990–7001.
35 S. S. Chen, I. K. M. Yu, D. W. Cho, H. Song, D. C. W. Tsang, J. P. Tessonnier, Y. S. Ok and C. S. Poon, *ACS Sustainable Chem. Eng*, 2018, **6**, 16113–16120.
36 I. K. M. Yu, X. Xiong, D. C. W. Tsang, L. Wang, A. J. Hunt, H. Song, J. Shang, Y. S. Ok and C. S. Poon, *Green Chem.*, 2019, **21**, 1267–1281.
37 M. Laiq Ur Rehman, Q. Hou, X. Bai, Y. Nie, H. Qian, T. Xia, R. Lai, G. Yu and M. Ju, *ACS Sustainable Chem. Eng*, 2022, **10**, 1986–1993.
38 P. Kenyon, D. W. J. Leung, Z. R. Turner, J. C. Buffet and D. O'Hare, *Macromolecules*, 2022, **55**, 3408–3414.

39 R. Trujillano, F. M. Labajos and V. Rives, *Appl. Clay Sci.*, 2023, **238**, 106927.
40 Y. Guo, Q. Zhang, Q. Hu, W. Tian, F. Leroux, P. Tang, D. Li and Y. Feng, *Mater. Today Commun.*, 2021, **29**, 102851.
41 C. Taviot-Guého, V. Prévot, C. Forano, G. Renaudin, C. Mousty and F. Leroux, *Adv. Funct. Mater.*, 2018, **28**, 1703868.
42 C. Forano, T. Hibino, F. Leroux and C. Taviot-Guého, *Dev. Clay Sci.*, 2006, **1**, 1021–1095.
43 V. Rives, *Mater. Chem. Phys.*, 2002, **75**, 19–25.
44 C. H. Zhou, J. N. Beltramini, C. X. Lin, Z. P. Xu, G. Q. Lu and A. Tanksale, *Catal. Sci. Technol.*, 2011, **1**, 111–122.
45 G. Varga, Á. Kukovecz, Z. Kónya, L. Korecz, S. Muráth, Z. Csendes, G. Peintler, S. Carlson, P. Sipos and I. Pálinkó, *J. Catal.*, 2016, **335**, 125–134.
46 I. Delidovich and R. Palkovits, *J. Catal.*, 2015, **327**, 1–9.
47 P. P. Upare, A. Chamas, J. H. Lee, J. C. Kim, S. K. Kwak, Y. K. Hwang and D. W. Hwang, *ACS Catal.*, 2020, **10**, 1388–1396.
48 M. Yabushita, N. Shibayama, K. Nakajima and A. Fukuoka, *ACS Catal.*, 2019, **9**, 2101–2109.
49 X. Ye, X. Shi, J. Li, B. Jin, J. Cheng, Z. Ren, H. Zhong, L. Chen, X. Liu, F. Jin and T. Wang, *Chem. Eng. J.*, 2022, **440**, 135844.
50 D. Kwon, J. Y. Kang, S. An, I. Yang and J. C. Jung, *J. Energy Chem.*, 2020, **46**, 229–236.
51 I. Delidovich and R. Palkovits, *ChemSusChem*, 2016, **9**, 547–561.
52 S. Park, D. Kwon, J. Y. Kang and J. C. Jung, *Green Energy Environ.*, 2019, **4**, 287–292.
53 G. Lee, Y. Jeong, A. Takagaki and J. C. Jung, *J. Mol. Catal. A: Chem.*, 2014, **393**, 289–295.
54 I. Delidovich and R. Palkovits, *Catal. Sci. Technol.*, 2014, **4**, 4322–4329.
55 S. Yu, E. Kim, S. Park, I. K. Song and J. C. Jung, *Catal. Commun.*, 2012, **29**, 63–67.
56 I. K. M. Yu, A. Hanif, D. C. W. Tsang, J. Shang, Z. Su, H. Song, Y. S. Ok and C. S. Poon, *Chem. Eng. J.*, 2020, **383**, 122914.
57 G. Varga, Z. Somosi, Z. Kónya, Á. Kukovecz, I. Pálinkó and I. Szilagyi, *J. Colloid Interface Sci.*, 2021, **581**, 928–938.
58 E. Géraud, S. Rafqah, M. Sarakha, C. Forano, V. Prevot and F. Leroux, *Chem. Mater.*, 2008, **20**, 1116–1125.
59 Y. J. Lin, D. Q. Li, D. G. Evans and X. Duan, *Polym. Degrad. Stab.*, 2005, **88**, 286–293.
60 E. Géraud, V. Prévot, J. Ghanbaja and F. Leroux, *Chem. Mater.*, 2006, **18**, 238–240.
61 I. Rousselot, C. Taviot-Guého, F. Leroux, P. Léone, P. Palvadeau and J. P. Besse, *J. Solid State Chem.*, 2002, **167**, 137–144.
62 M. Yang, E. Tuckley, J. C. Buffet and D. O'Hare, *J. Mater. Chem. A*, 2015, **4**, 500–504.
63 J. Y. Lee, G. H. Gwak, H. M. Kim, T. Il Kim, G. J. Lee and J. M. Oh, *Appl. Clay Sci.*, 2016, **134**, 44–49.
64 Q. Wang, H. H. Tay, Z. Guo, L. Chen, Y. Liu, J. Chang, Z. Zhong, J. Luo and A. Borgna, *Appl. Clay Sci.*, 2012, **55**, 18–26.
65 D. G. Cantrell, L. J. Gillie, A. F. Lee and K. Wilson, *Appl. Catal., A*, 2005, **287**, 183–190.
66 D. Tichit, M. Naciri Bennani, F. Figueras, R. Tessier and J. Kervennal, *Appl. Clay Sci.*, 1998, **13**, 401–415.
67 I. Pálinkó, P. Sipos, O. Berkesi and G. Varga, *J. Phys. Chem. C*, 2022, **126**, 15254–15262.
68 D. W. J. Leung, C. Chen, J. C. Buffet and D. O'Hare, *Dalton Trans.*, 2020, **49**, 9306–9311.
69 M. G. Álvarez, R. J. Chimentão, F. Figueras and F. Medina, *Appl. Clay Sci.*, 2012, **58**, 16–24.
70 J. S. Valente, H. Pfeiffer, E. Lima, J. Prince and J. Flores, *J. Catal.*, 2011, **279**, 196–204.
71 F. M. P. R. van Laar, D. E. De Vos, P. A. Jacobs, F. Pierard, A. Kirsch-De Mesmaeker and L. Fiermans, *J. Catal.*, 2001, **197**, 139–150.
72 S. Muráth, T. Varga, A. Kukovecz, Z. Kónya, P. Sipos, I. Pálinkó and G. Varga, *Mater. Today Chem.*, 2022, **23**, 100682.
73 A. A. Marianou, C. M. Michailof, A. Pineda, E. F. Iliopoulou, K. S. Triantafyllidis and A. A. Lappas, *ChemCatChem*, 2016, **8**, 1100–1110.
74 C. Chen, K. Ruengkajorn, J. C. Buffet and D. O'Hare, *RSC Adv.*, 2018, **8**, 34650–34655.
75 M. Pavlovic, P. Rouster, T. Oncsik and I. Szilagyi, *ChemPlusChem*, 2017, **82**, 121–131.
76 M. Pavlovic, R. Huber, M. Adok-Sipiczki, C. Nardin and I. Szilagyi, *Soft Matter*, 2016, **12**, 4024–4033.
77 Z. Gu, J. J. Atherton and Z. P. Xu, *Chem. Commun.*, 2015, **51**, 3024–3036.
78 Z. P. Xu and P. S. Braterman, *J. Phys. Chem. C*, 2007, **111**, 4021–4026.
79 N. E. H. Hadj-Abdelkader, A. P. Beltrao-Nunes, F. Belkhadem, N. Benselka, R. Roy and A. Azzouz, *Appl. Clay Sci.*, 2020, **198**, 105829.
80 M. Yabushita, H. Kobayashi, J. Y. Hasegawa, K. Hara and A. Fukuoka, *ChemSusChem*, 2014, **7**, 1443–1450.
81 Z. P. Xu, G. Stevenson, C. Q. Lu and G. Q. Lu, *J. Phys. Chem. B*, 2006, **110**, 16923–16929.
82 Y. Zhao, F. Li, R. Zhang, D. G. Evans and X. Duan, *Chem. Mater.*, 2002, **14**, 4286–4291.
83 K. J. Martin and T. J. Pinnavaia, *J. Am. Chem. Soc.*, 1986, **108**, 541–542.
84 V. R. L. Constantino and T. J. Pinnavaia, *Inorg. Chem.*, 1995, **34**, 883–892.